Modeling, Simulation, and Control of Parachute/Balloon Flight Systems for Mars Exploration (DRAFT PAPER)

Marco B. Quadrelli*, Jonathan M. Cameron*, and Viktor Kerzhanovich*

Abstract— **In this paper, we report some models developed for analyzing Parachute/Balloon-assisted deployment of sensor packages within the Mars Aerobot Validation Program (MABVAP) at JPL. Two different scenarios are described: pointing dynamics and control of an articulated payload mounted on a superpressure balloon-supported gondola, and the dynamics of various flight train configurations with parachute and superpressure balloons in different geometries and oscillatory regimes originated upon deployment. These scenarios have been motivated by the need to predict and validate flight-train stability behavior upon deployment before and after tests have been made.**

Keywords— **aerodynamic decelerator, parachute, balloon, deployment, dynamics, control, pointing**

Introduction

In the following, we document the analysis, and testing done to assess the validity of models developed for Parachute/Balloon-assisted deployment of sensor packages within the Mars Aerobot Validation program at JPL. Two main scenarios are described.

On the first scenario, we analyze the pointing dynamics and control of an articulated payload mounted on a balloon-supported gondola. An analysis has been made to verify the feasibility of tracking an inertially fixed point from a gimballed payload aboard a floating aerobot. The equations of motion and control laws are described, as well as numerical results obtained for different configurations which cover a domain in a parameter space defined in terms of wind gust profiles, tether lengths, balloon diameters, and gondola/camera inertia properties. A parametric plot is obtained that shows typical trends to be expected as a function of those parameters.

On the second scenario, models and analytical simulations are reported to predict and validate the dynamics of various flight train configurations in different oscillatory regimes originated upon deployment. Qualitative correlations with experimental data are also reported. The geometric arrangements described by these models include: a balloon tethered in wind tunnel, a balloon tethered to a parachute in wind tunnel, a balloon tethered to a gondola in free fall, a balloon tethered to a parachute and to a gondola in free-fall, descent of a gondola under an inflating balloon still connected to a parachute. A model is also proposed to capture the interaction of the airflow with the deformable surface of a partially inflated balloon. The intent of these models is to determine the onset of dynamic oscillatory instability (presumably attributed to von Karman vortex shedding) of the balloon as a function of design parameters such as: parachute diameters and riser length, balloon diameter, balloon-gondola tether length, gondola mass and inertia.

These scenarios have been motivated by the need to predict and validate flight-train stability behavior upon deployment before and after tests have been made. Both wind tunnel tests and drop tests have been conducted, at NASA LaRC and Glenn, and at JPL, under the direction of the third author. These tests are reported in detail in another paper [3].

* Member of Technical Staff, Guidance & Control, Analysis Section, Mail Stop 198-326, Jet Propulsion Laboratory, 4800 Oak Grove Drive, Pasadena, CA 91109-8099, phone (818) 354-7548, fax (818) 393-4440, marco@grover.jpl.nasa.gov

* Member of Technical Staff, Guidance & Control, Analysis Section, Jet Propulsion Laboratory

* Member of Technical Staff, Avionic Systems Engineering Section, Jet Propulsion Laboratory

I. First Scenario: Payload Pointing Dynamics from Balloon suspended Gondola

A. Analytical Models

A.1 Modeling Assumptions

The assumptions of the model are as follows:

- The reference frames of interest are the inertial frame (or planet frame), and the gondola (or body-fixed) frame. The gondola is taken here to be the preferential body, contrary to common balloon dynamics usage which places the body frame at the balloon, because sensors and actuators are located on the gondola, rather than the balloon.
- The inertial coordinate frame N is denoted by the triad $\mathcal{F}_\backslash = (\mathbf{n_1}, \mathbf{n_2}, \mathbf{n_3})$, and the gondola body frame G by $\mathcal{F}_| = (\mathbf{b_1}, \mathbf{b_2}, \mathbf{b_3})$.
- The translational dynamics is measured in N, while the rotational dynamics of the gondola and all the other bodies of the serial chain are measured in G.
- The camera P and the gondola G are modelled as rigid bodies.
- The tether connecting the gondola to the balloon is modelled as a viscoelastic continuum, and discretized into N lumped masses.
- The balloon, considered to be a fully inflated rigid sphere, is modelled as a point mass, and constitutes point mass number $N+1$ of the tether.
- The attitude of the gondola G is stabilized by a set of three reaction wheels, W1, W2, and W3, located at the center of mass of G and whose spin axes are directed along the principal axes of G.
- The camera P is connected to G through a universal joint (U-joint), allowing two rotational degrees of freedom (θ and ϕ) for the relative motion of P with respect to G.
- The balloon is subject to gravity and to a constant flow of air in the $\mathbf{i_3}$ direction.

• The balloon may be connected to a gondola by a rigid link representing a cable.
• The balloon is represented by a point mass or by a rigid sphere. Partial inflation of the envelope is a very difficult thing to model, since it implies a deformable envelope, so we assume the balloon is 100% full. However, the gas inside the envelope is a partial mixture of the percentage of Helium a_{He}, and of the percentage of air a_{air}. Given the gas constants of He and air ($R_{He} = R0/\mu_{He} = 2077.15J/(Kg°K)$ and $R_{air} = R0/\mu_{air} = 286.06J/(Kg°K)$, where the molecular weights are $\mu_{He} = 4.003$ and $\mu_{air} = 28.97$ and $R0 = 8314J/(Kg°K)$), the densities are given by the equations:

$$\rho_{He} = \frac{p_0}{R_{He}T_0} \quad (1)$$

$$\rho_{air} = \frac{p_0}{R_{air}T_0} \quad (2)$$

the masses are given by:

$$M_{He} = a_{He}V\rho_{He} \quad (3)$$

$$M_{air} = (1 - a_{He})V\rho_{air} \quad (4)$$

where V is the volume of the balloon sphere, and the total mass of gas inside the envelope is $M_{He} + M_{air}$. If M_{env} is the mass of the material of the envelope, and M_{added} is the added mass of air caused by the fact that the balloon moves in a fluid, we have that the total balloon mass is:

$$M_{tot} = M_{He} + M_{air} + M_{env} + M_{added} \quad (5)$$

where

$$M_{added} = 0.5\rho_{air}V \quad (6)$$

The buoyancy vector is given by:

$$Buo = (\rho Vg - (M_{He} + M_{air})g)\mathbf{i_3} \quad (7)$$

and the effective lift vector is

$$Lift = (Buo - m_{env}g)\mathbf{i_3} \quad (8)$$

• The drag on the balloon is represented by

$$D_b = 1/2\rho_{air}V_b^2CD_bS_b \quad (9)$$

with drag coefficient $CD_b = 0.4$, balloon frontal area S_b, and the center of mass velocity is equal to:

$$V_b = \sqrt{(\dot{x_b} - U_x)^2 + (\dot{y_b} - U_y)^2} \quad (10)$$

where U_i is the (absolute) component of the airflow in the i-th direction.
• There is no lift acting on the balloon. However, an unsteady force acts on the balloon perpendicular to the direction of the relative flow, and is caused by the vortex detachment behind the balloon. As such, this force is called the Strouhal force. It is given by:

$$S_b = 1/2\rho_{air}V_b^2CD_bS_bsin(2\pi\nu t)$$

where

$$St = \frac{\nu D_b}{V}$$

is the Strouhal number. For the balloon, it is assumed to be equal to 0.2. The sinusoidal term is the simplest representation of the unsteady behavior, which in a more realistic model would contain higher harmonics.

A.2 Kinematics

• The translational dynamics of G is parameterized in terms of the linear velocity components of its center of mass $G+$ as

$${}^{N}\mathbf{v}^{\mathbf{G+}} = (\dot{\mathbf{x}}, \dot{\mathbf{y}}, \dot{\mathbf{z}})\mathcal{F}_{\backslash} \quad (11)$$

and the rotational dynamics as

$${}^{N}\boldsymbol{\omega}^{\mathbf{G}} = (\boldsymbol{\omega_1}, \boldsymbol{\omega_2}, \boldsymbol{\omega_3})\mathcal{F}_{\lfloor} \quad (12)$$

• The translational dynamics of each tether point P_i is parameterized in terms of the linear velocity components of its center of mass as

$${}^{N}\mathbf{v}^{\mathbf{P_i}} = (\dot{\mathbf{x}}_\mathbf{i}, \dot{\mathbf{y}}_\mathbf{i}, \dot{\mathbf{z}}_\mathbf{i})\mathcal{F}_{\backslash} \quad (13)$$

• The rotational dynamics of each wheel Wi is parameterized as

$${}^{G}\boldsymbol{\omega}^{\mathbf{W_i}} = \boldsymbol{\Omega_i}\mathbf{a_i} \quad (14)$$

where Ω_i is the spin rate of the wheel with respect to the gondola, and $\mathbf{a_i}$ denotes the direction of the spin axis in $\mathcal{F}_{\lfloor}$ (here, $\mathbf{a_i} = \mathbf{b_i}$).
• The translational dynamics of the camera P is parameterized in terms of the linear velocity components of its center of mass $P+$ as

$${}^{N}\mathbf{v}^{\mathbf{P+}} = {}^{\mathbf{N}}\mathbf{v}^{\mathbf{G+}} + {}^{\mathbf{N}}\boldsymbol{\omega}^{\mathbf{G}} \times \mathbf{l} + {}^{\mathbf{N}}\boldsymbol{\omega}^{\mathbf{P}} \times \mathbf{r} \quad (15)$$

and its rotational dynamics as

$${}^{N}\boldsymbol{\omega}^{\mathbf{P}} = {}^{\mathbf{N}}\boldsymbol{\omega}^{\mathbf{G}} + (\dot{\boldsymbol{\phi}}\mathbf{s}\boldsymbol{\theta}, -\dot{\boldsymbol{\phi}}\mathbf{c}\boldsymbol{\theta}, \dot{\boldsymbol{\theta}})\mathcal{F}_{\lfloor} \quad (16)$$

where $s = sin$ and $c = cos$.
• The wind velocity vector is represented as

$$\mathbf{W_{wind}} = (\mathbf{W_x}, \mathbf{W_y}, \mathbf{W_z})\mathcal{F}_{\backslash} \quad (17)$$

• Other points of interest for the kinematics are the camera connection point Q and the tether connection point H1, for which

$${}^{N}\mathbf{v}^{\mathbf{Q}} = {}^{\mathbf{N}}\mathbf{v}^{\mathbf{G+}} + {}^{\mathbf{N}}\boldsymbol{\omega}^{\mathbf{G}} \times \mathbf{l}^{\mathbf{N}}\mathbf{v}^{\mathbf{H_1}} = {}^{\mathbf{N}}\mathbf{v}^{\mathbf{G+}} + {}^{\mathbf{N}}\boldsymbol{\omega}^{\mathbf{G}} \times \mathbf{d} \quad (18)$$

• The accelerations of all these points are denoted by $\mathbf{a}$, whereas the angular acceleration of frames is denoted by $\boldsymbol{\alpha}$.

A.3 System Equations of Motion

We adopt a projection method to derive the equations of motion. This method has the advantage that it directly leads to a set of equations which are easily coded in symbolic form, and they are all written in terms of the velocities. The total number of bodies forming the gondola-camera-wheels-tether-balloon system is $nbod = 6 + N_p$,

where N_p is the number of tether points. The total number of configuration degrees of freedom is $ndof = 7+2+3+3\cdot N_p+3$, where the attitude of the gondola is parameterized in terms of the quaternion vector. The total number of motion degrees of freedom is $ndof = 6+2+3+3\cdot N_p+3$. We therefore identify the following generalized velocities for the problem: $\dot{x},\dot{y},\dot{z},\omega_1,\omega_2,\omega_3,\ \Omega_1,\Omega_2,\Omega_3,\dot{\theta},\dot{\phi},\ \dot{x}_1,\dot{y}_1,\dot{z}_1,\dot{x}_2,\dot{y}_2,\dot{z}_2,...,\dot{x}_N,\dot{y}_N,\dot{z}_N,\dot{x}_{N+1},\dot{y}_{N+1},\dot{z}_{N+1}$. Consequently, the vector of generalized inertia forces, namely, the vector of inertial, Coriolis, and centrifugal forces (i.e., the left hand side of the equations of motion) can be written as follows (r denotes the equation number):

$$
\begin{aligned}
F_r^{inertial} = \\
&(m_G+\sum_i^{Nw} m_{W_i})\,{}^N\mathbf{a}^{\mathbf{G}+}\cdot{}^N\mathbf{v}_\mathbf{r}^{\mathbf{G}+} + \\
&m_P\,{}^N\mathbf{a}^{\mathbf{P}+}\cdot{}^N\mathbf{v}_\mathbf{r}^{\mathbf{P}+} + \\
&\sum_i^{Np} m_i\,{}^N\mathbf{a}^{\mathbf{i}}\cdot{}^N\mathbf{v}_\mathbf{r}^{\mathbf{i}} + \\
&{}^N\boldsymbol{\omega}_\mathbf{r}^{\mathbf{P}}\cdot(\mathbf{J_P}\,{}^N\boldsymbol{\alpha}^{\mathbf{P}}+{}^N\boldsymbol{\omega}^{\mathbf{G}}\times\mathbf{J_P}\,{}^N\boldsymbol{\omega}^{\mathbf{P}}) + \\
&\sum_i^{Nw}{}^G\boldsymbol{\omega}_\mathbf{r}^{\mathbf{W_i}}\cdot[\mathbf{J_i}({}^N\boldsymbol{\alpha}^{\mathbf{G}}+{}^N\dot{\boldsymbol{\Omega}}^{\mathbf{W_i}}) + \\
&{}^N\boldsymbol{\omega}^{\mathbf{G}}\times\mathbf{J_i}({}^N\boldsymbol{\omega}^{\mathbf{G}}+{}^G\boldsymbol{\Omega}^{\mathbf{W_i}})] + \\
&{}^N\boldsymbol{\omega}_\mathbf{r}^{\mathbf{G}}\cdot\{(\mathbf{J_G}+\sum_\mathbf{i}^{\mathbf{Nw}}\mathbf{J_i})\,{}^N\boldsymbol{\alpha}^{\mathbf{G}}\} + \\
&{}^N\boldsymbol{\omega}_\mathbf{r}^{\mathbf{G}}\cdot\{{}^N\boldsymbol{\omega}^{\mathbf{G}}\times[(\mathbf{J_G}+\sum_\mathbf{i}^{\mathbf{Nw}}\mathbf{J_i})\,{}^N\boldsymbol{\omega}^{\mathbf{G}}]\} + \\
&{}^N\boldsymbol{\omega}_\mathbf{r}^{\mathbf{G}}\cdot\{\sum_i^{Nw}[(\mathbf{J_i}\,{}^G\dot{\boldsymbol{\Omega}}^{\mathbf{i}}+{}^N\boldsymbol{\omega}^{\mathbf{G}}\times\mathbf{J_i}\,{}^G\boldsymbol{\Omega}^{\mathbf{i}})]\}
\end{aligned}
$$

from which the system inertia matrix and nonlinear terms can be derived. In sequence, the first three lines represent the contribution of the translational terms of the gondola, camera, and tether points, respectively. The fourth, fifth, and sixth lines represent the contribution of the rotational terms of the camera, gondola, and reaction wheels, respectively. The $(r-th, s-th)$ entry of the inertia matrix is given by:

$$
\begin{aligned}
M_{rs} = &(m_G+\sum_i^{Nw} m_{W_i})\,{}^N\mathbf{v}_\mathbf{r}^{\mathbf{G}+}\cdot{}^N\mathbf{v}_\mathbf{s}^{\mathbf{G}+} + \\
&m_P\,{}^N\mathbf{v}_\mathbf{r}^{\mathbf{P}+}\cdot{}^N\mathbf{v}_\mathbf{s}^{\mathbf{P}+} + \\
&\sum_i^{Np} m_i\,{}^N\mathbf{v}_\mathbf{r}^{\mathbf{i}}\cdot{}^N\mathbf{v}_\mathbf{s}^{\mathbf{i}} + \\
&{}^N\boldsymbol{\omega}_\mathbf{r}^{\mathbf{P}}\cdot\mathbf{J_P}\,{}^N\boldsymbol{\omega}_\mathbf{s}^{\mathbf{P}} \\
&\sum_i^{Nw}{}^G\boldsymbol{\omega}_\mathbf{r}^{\mathbf{W_i}}\cdot[\mathbf{J_i}({}^N\boldsymbol{\omega}_\mathbf{s}^{\mathbf{G}}+{}^G\boldsymbol{\Omega}_\mathbf{s}^{\mathbf{W_i}})] + \\
&{}^N\boldsymbol{\omega}_\mathbf{r}^{\mathbf{G}}\cdot\{(\mathbf{J_G}+\sum_\mathbf{i}^{\mathbf{Nw}}\mathbf{J_i})\,{}^N\boldsymbol{\omega}_\mathbf{s}^{\mathbf{G}}+\sum_\mathbf{i}^{\mathbf{Nw}}\mathbf{J_i}\,{}^G\boldsymbol{\Omega}_\mathbf{s}^{\mathbf{W_i}}]\}
\end{aligned}
$$

where the indeces r and s run over the set of generalized velocities, and where the indexed speed denotes a *partial velocity* (${}^N\mathbf{v}_\mathbf{r}^{\mathbf{G}+}$ for instance, represents the partial derivative of ${}^N\mathbf{v}^{\mathbf{G}+}$ in the direction of the $r-th$ generalized velocity). The $r-th$ component of the vector of gyroscopic (i.e., Coriolis and centrifugal) terms is given by:

$$
\begin{aligned}
F_r^{nonlinear} = &(m_G+\sum_i^{Nw} m_{W_i})\,{}^N\mathbf{a}_\mathbf{t}^{\mathbf{G}+}\cdot{}^N\mathbf{v}_\mathbf{r}^{\mathbf{G}+} + \\
&m_P\,{}^N\mathbf{a}_\mathbf{t}^{\mathbf{P}+}\cdot{}^N\mathbf{v}_\mathbf{r}^{\mathbf{P}+} + \\
&\sum_i^{Np} m_i\,{}^N\mathbf{a}_\mathbf{t}^{\mathbf{i}}\cdot{}^N\mathbf{v}_\mathbf{r}^{\mathbf{i}} + \\
&{}^N\boldsymbol{\omega}_\mathbf{r}^{\mathbf{P}}\cdot(\mathbf{J_P}\,{}^N\boldsymbol{\alpha}_\mathbf{t}^{\mathbf{P}}+{}^N\boldsymbol{\omega}^{\mathbf{G}}\times\mathbf{J_P}\,{}^N\boldsymbol{\omega}^{\mathbf{P}}) + \\
&\sum_i^{Nw}{}^G\boldsymbol{\omega}_\mathbf{r}^{\mathbf{W_i}}\cdot[\mathbf{J_i}({}^N\boldsymbol{\alpha}_\mathbf{t}^{\mathbf{G}}+{}^N\dot{\boldsymbol{\Omega}}_\mathbf{t}^{\mathbf{W_i}}) + \\
&{}^N\boldsymbol{\omega}^{\mathbf{G}}\times\mathbf{J_i}({}^N\boldsymbol{\omega}^{\mathbf{G}}+{}^G\boldsymbol{\Omega}^{\mathbf{W_i}})] + \\
&{}^N\boldsymbol{\omega}_\mathbf{r}^{\mathbf{G}}\cdot\{(\mathbf{J_G}+\sum_\mathbf{i}^{\mathbf{Nw}}\mathbf{J_i})\,{}^N\boldsymbol{\alpha}_\mathbf{t}^{\mathbf{G}} + \\
&{}^N\boldsymbol{\omega}^{\mathbf{G}}\times[(\mathbf{J_G}+\sum_\mathbf{i}^{\mathbf{Nw}}\mathbf{J_i})\,{}^N\boldsymbol{\omega}^{\mathbf{G}}] + \\
&\sum_i^{Nw}[(\mathbf{J_i}\,{}^G\dot{\boldsymbol{\Omega}}_\mathbf{t}^{\mathbf{i}}+{}^N\boldsymbol{\omega}^{\mathbf{G}}\times\mathbf{J_i}\,{}^G\boldsymbol{\Omega}^{\mathbf{i}})]\}
\end{aligned}
$$

where the subscript $(\cdot)_t$ denotes the contribution of that acceleration to the nonlinear terms (at least quadratic in the velocities).

From the above information, we obtain the partial velocities ${}^N\mathbf{v}_\mathbf{r}^{\mathbf{G}+}$, ${}^N\mathbf{v}_\mathbf{r}^{\mathbf{Q}}$, ${}^N\mathbf{v}_\mathbf{r}^{\mathbf{H1}}$, ${}^N\mathbf{v}_\mathbf{r}^{\mathbf{P}+}$, ${}^N\mathbf{v}_\mathbf{r}^{\mathbf{i}}$, ${}^N\boldsymbol{\omega}_\mathbf{r}{}^{\mathbf{G}}$, ${}^N\boldsymbol{\omega}_\mathbf{r}{}^{\mathbf{W_1}}$, ${}^N\boldsymbol{\omega}_\mathbf{r}{}^{\mathbf{W_2}}$, ${}^N\boldsymbol{\omega}_\mathbf{r}{}^{\mathbf{W_3}}$, ${}^N\boldsymbol{\omega}_\mathbf{r}{}^{\mathbf{P}}$, where r=1,...11+i+2, and $i=1,...,N_p$.Also, we use the notation $z_1 = l_1 + hc\theta c\phi$, $z_2 = l_2 + hs\theta c\phi$, $z_3 = l_3 + hs\phi$, $gt_1 = -hs\theta c\phi$, $gt_2 = +hc\theta c\phi$, $gf_1 = -hc\theta s\phi$, $gf_2 = -hs\theta s\phi$, $gf_3 = +hc\phi$, and h represents the distance from the center of the U-joint to the center of mass of the camera.

The vector of generalized external forces can be written in component form by bringing into evidence the velocities of each point of force application and the angular velocity of each frame of reference where a torque is applied. We obtain:

$$
\begin{aligned}
F_r^{external} = &(\mathbf{W_g}+\mathbf{F}_{\mathbf{g_{aero}}})\cdot{}^N\mathbf{v}_\mathbf{r}^{\mathbf{G}+} + \\
&(\mathbf{T_1})\cdot{}^N\mathbf{v}_\mathbf{r}^{\mathbf{H_1}} + \\
&(\mathbf{W_p})\cdot{}^N\mathbf{v}_\mathbf{r}^{\mathbf{P}+} + \\
&\sum_i^{Np}(\mathbf{W_i}+\mathbf{F}_{\mathbf{i_{aero}}}+\mathbf{T_i}-\mathbf{T_{i-1}})\cdot{}^N\mathbf{v}_\mathbf{r}^{\mathbf{i}} + \\
&(\mathbf{W}_{\mathbf{N_p+1}}+\mathbf{F}_{\mathbf{N_p+1_{aero}}})\cdot{}^N\mathbf{v}_\mathbf{r}^{\mathbf{N_p+1}} + \\
&(\mathbf{B_b}-\mathbf{T}_{\mathbf{N_p+1}})\cdot{}^N\mathbf{v}_\mathbf{r}^{\mathbf{N_p+1}} + \\
&(\tau_\phi s\theta,-\tau_\phi c\theta,\tau_\theta)\mathcal{F}_\lfloor\cdot{}^N\boldsymbol{\omega}_\mathbf{r}^{\mathbf{P}} + \\
&\sum_i^{Nw}(\boldsymbol{\tau}_{\mathbf{wi}})\cdot{}^G\boldsymbol{\omega}_\mathbf{r}^{\mathbf{W_i}} +
\end{aligned}
$$

$$[-\boldsymbol{\tau}_{\mathbf{w1}} - \boldsymbol{\tau}_{\mathbf{w2}} - \boldsymbol{\tau}_{\mathbf{w3}}] \cdot {}^{\mathbf{N}}\boldsymbol{\omega}_{\mathbf{r}}^{\mathbf{G}} - [(\tau_\phi s\theta, -\tau_\phi c\theta, \tau_\theta)\mathcal{F}_{\lfloor}] \cdot {}^{N}\boldsymbol{\omega}_{\mathbf{r}}^{\mathbf{G}}$$

where $\mathbf{W_g}$, $\mathbf{W_p}$, and $\mathbf{W_i}$ for $i = 1, ..., N_p$ are the weights, $\mathbf{F_{g_{aero}}}$ and $\mathbf{F_{i_{aero}}}$ are the aerodynamic forces acting on the center of mass (there should also be an aerodynamic moment, which we neglect in this analysis), $\mathbf{T_i}$ is the tether tension in the $i-th$ link, $\mathbf{B_b}$ is the balloon buoyancy force, $\boldsymbol{\tau}_{\mathbf{wj}}$, for $j = 1, 2, 3$ are the reaction wheel command torques, and τ_θ and τ_ϕ are the camera command torques in the θ and ϕ directions, respectively.

B. Stochastic Wind Model

In order to generate wind data that is representative of typical planetary winds that a balloon might encounter, we developed a stochastic wind model based on first order markov model. See Bryson and Ho for details [?, p.328–335]. For this model, we assume that the varying winds can be represented in the following form:

$$\dot{v}(t) = -\beta v(t) + \sigma_{\text{N}} w(t) \tag{19}$$

where $w(t)$ is a zero-mean, unity variance, white noise process with the following characteristics:

$$\text{E}\left[w(t)\right] = \overline{w}(t) = 0 \tag{20}$$

$$\text{E}\left[w(t)^2\right] = 1 \tag{21}$$

The solution for Equation 19 involves the usual transition matrix, $\Phi(\Delta t)$:

$$\Phi(t, t + \Delta t) = \Phi(\Delta t) = e^{-\beta \Delta t} \tag{22}$$

Consulting Bryson and Ho, we want to get our wind model equation into the following form:

$$\dot{x}(t) = F(t)x(t) + G(t)w(t) \tag{23}$$

where $w(t)$ is also a zero-mean, unity variance, white noise process. Comparing with Equation 19, we see that:

$$x(t) = v(t) \tag{24}$$

$$F(t) = -\beta \tag{25}$$

$$G(t) = \sigma_{\text{N}} \tag{26}$$

The covariance of state $x(t)$ is defined as $X(t)$:

$$X(t) = \text{E}\left[(x(t) - \overline{x}(t))^2\right] \tag{27}$$

The evolution of the state covariance can now be expressed:

$$\dot{X}(t) = F(t)X(T) + X(t)F(t)^T + G(t)Q(t)G(t) \tag{28}$$

where $Q(t)$ is the covariance of the white noise process. Since this is a stationary process and the state is scalar, the following simple differential equation results:

$$\dot{X}(t) = -2\beta X(t) + \sigma_{\text{N}}^2 \tag{29}$$

where $Q(t) = q = 1$. The solution to this equation is straightforward:

$$X(t) = \frac{\sigma_{\text{N}}^2}{2\beta}\left(1 - e^{-2\beta t}\right) \tag{30}$$

Since this is a stationary process, $X(t)$ will approach some final value as time increases and $\dot{X}(t)$ will approach zero. So as time increases:

$$\text{as} \quad t \to \infty, \quad X(t) \to \frac{\sigma_{\text{N}}^2}{2\beta} \tag{31}$$

Recalling the definition of $X(t) = \text{E}\left[(x(t) - \overline{x}(t))^2\right] = \text{E}\left[(v(t) - \overline{v}(t))^2\right]$, the limiting value for $X(t)$ is σ_{V}^2. Therefore it is clear that:

$$\sigma_{\text{V}}^2 = \frac{\sigma_{\text{N}}^2}{2\beta} \tag{32}$$

from which we see that the necessary scaling for the white noise process is:

$$\sigma_{\text{N}} = \sqrt{2\beta}\,\sigma_{\text{V}} \tag{33}$$

B.1 Discrete approximations

Unfortunately, using the simple differential equation for the wind noise model in most modern adaptive integrators will produce significant computational "thrashing". The reason behind this is that the white noise process $w(t)$ must be approximated by calling a gaussian random number generator. This means the right hand side of the governing differential equation (Equation 19) will not reproduce the same value as t aproaches some specific time (t_k) in the limit (because no two samplings of $w(t_k)$ will produce the same number).

In order to deal with this difficulty, it is necessary to convert the continuous differential equation in $v(t)$ into a discrete time step version[1]:

$$x_{k+1} = \Phi(\Delta t)x_k + \xi_k \tag{34}$$

where $x_k = x(t_k)$ and $t_{k+1} = t_k + \Delta t$, and ξ_k is the contribution of the white noise process over the interval:

$$\xi_k = \int_{t_k}^{t_{k+1}} \Phi(t_{k+1} - t)\sigma_{\text{N}} w(\tau) dt \tag{35}$$

Unfortunately, we do not have access to a real white noise process, $w(k)$. We must approximate it with a zero mean, unity variance, randomly generated, number w_k. So the question remains, how should this number be scaled over the interval to approximate the effect of the true white noise process, $w(k)$, over the interval. Assuming only one sampling of the w_k is available in the interval, it seems clear that:

$$\xi_k = \sqrt{\text{E}\left[\xi_k^2\right]}\, w_k \tag{36}$$

where the expected value of the square of ξ_k over the interval is:

$$\text{E}\left[\xi_k^2\right] = \int_{t_k}^{t_{k+1}} \Phi^2(t_{k+1} - t)\sigma_{\text{N}}^2 \text{E}\left[(w(t) - \overline{w}(t))^2\right] dt \tag{37}$$

[1] See the gyro model analysis for the Cassini spacecraft [?, Section 9.3, p.7–8] for a similar analysis.

Recalling that the white noise process is unity variance, $\mathrm{E}\left[(w(t)-\overline{w}(t))^2\right]=1$. Converting the integrating variable by letting $\tau = t_{k+1}-t$, the integral becomes:

$$\mathrm{E}\left[\xi_k^2\right] = \sigma_{\mathrm{N}}^2\int_{\Delta t}^{0}(\Phi(\tau))^2(-d\tau) \quad (38)$$

$$= \sigma_{\mathrm{N}}^2\int_{0}^{\Delta t}e^{-2\beta\tau}d\tau \quad (39)$$

$$= -\frac{\sigma_{\mathrm{N}}^2}{2\beta}\left[e^{-2\beta\tau}\right]_0^{\Delta t} \quad (40)$$

$$= -\frac{\sigma_{\mathrm{N}}^2}{2\beta}\left(e^{-2\beta\Delta t}-1\right) \quad (41)$$

However, since Δt is small, a first order approximation for the last term can be applied:

$$e^{-2\beta\Delta t}-1\approx -2\beta\Delta t \quad (42)$$

Therefore:

$$\mathrm{E}\left[\xi_k^2\right] = -\left(\frac{\sigma_{\mathrm{N}}^2}{2\beta}\right)(-2\beta\Delta t) \quad (43)$$

$$= \sigma_{\mathrm{N}}^2\Delta t \quad (44)$$

Therefore, the exected contribution of the white noise process over the interval Δt is:

$$\xi_k = \sqrt{\mathrm{E}\left[\xi_k^2\right]} = \sigma_{\mathrm{N}}\sqrt{\Delta t} \quad (45)$$

Finally, the discrete update equation needed is:

$$x_{k+1} = e^{-\beta\Delta t}x_k + \sigma_{\mathrm{N}}\sqrt{\Delta t}\,w_k \quad (46)$$

Since Δt is small, the first order approximation $e^{-\beta\Delta t}\approx(1-\beta\Delta t)$, we have a simple Euler integration scheme:

$$x_{k+1} = x_k - \beta x_k\Delta t + \sqrt{2\beta\Delta t}\,\sigma_{\mathrm{V}}\,w_k \quad (47)$$

where σ_{N} has been replaced by $\sigma_{\mathrm{N}}=\sqrt{2\beta}\,\sigma_{\mathrm{V}}$.

Although this update equation can be used as part of a user-defined fixed-step integration routine, perhaps a better approach is to use this exact scheme to generate a set of wind data having the desired characteristics. Then use that synthetic wind data (with associated time information) to construct a function $W(t)$ that will do a table lookup in the previously generated wind data, interpolate if desired, and return the wind at the specified time. This function can be used directly with adaptive integration routines because the values are reproduceable for a specific t_k and approach the same value as t_k is approached from either side.

B.2 Extracting stochastic parameters from wind data

In order to construct simulated wind data that has similar characteristics to actual wind data, it is necessary to analyze actual data and extract two parameters, the standard deviation of the wind velocity (σ_{V}), and the *autocorrelation time*, T_{V}. The parameter β in the differential equation governing the random wind speed model (Equation 19) is defined to be the reciprocal of the correlation time:

$$\beta = \frac{1}{T_{\mathrm{V}}} \quad (48)$$

The meaning of the correlation time is that the wind velocity is not highly autocorrelated beyond much more than the correlation time.

Assume that we have a set of N wind velocity samples, v_i, sampled at time intervals of Δt_v. Getting the standard deviation of the wind velocity requires a simple statistical analysis:

$$\sigma_{\mathrm{V}}^2 = \frac{1}{N-1}\sum_{i=1}^{N}(v_i-\overline{v})^2 \quad (49)$$

where $\overline{v}$ is the mean of the wind velocity values.

Determining the autocorrelation time requires more analysis. First, define the autocorrelation function $f(k)$:

$$f(k) = \frac{1}{N-k-1}\sum_{i=1}^{N-k}(v_i-\overline{v})(v_{i+k}-\overline{v}) \quad (50)$$

This function correlates the data with a shifted version of itself in a root-mean-square sense. If $k=0$, $f(k)$ should reproduce the variance of the data. If $k=1$, $f(k)$ should give the correlation of the data with the data shifted one time step, Δt_v. As k increases, the autocorrelation should decrease exponentially. Apply the autocorrelation function for various k to determine how large k has to get for the values of $f(k)$ to be small. Let K be the necessary value of k for $f(k)$ to be as small as desired. Now construct a set of data pairs $(t_k, f(k))$ from $k=0$ through K where $t_k = k\Delta t$. Plotting the result will produce an autocorrelation plot. Figure ?? shows an example autocorrelation plot of some sampled data. To determine the autocorrelation time from the autocorrelation data, it is necessary to fit the data to an exponential function:

$$Ae^{-t_k/T_{\mathrm{V}}} \quad (51)$$

The resulting estimate of T_{V} will be a good approximation of the autocorrelation time and its reciprocal is the desired β necessary for the wind model.

C. Pointing Control Algorithms

The pointing control algorithms developed for this study rely on a feedback linearization of the dynamics to derive a globally, exponentially stable controller for the pointing dynamics. The actuators considered are a set of three reaction wheels, of sizes consistent with those used in scientific ballooning experiments. The reaction wheels operate about the nominal attitude of the gondola, and provide three-axis stabilization of the reference body triad from which the pointing payload (camera) operates. The payload is hinged at a bottom location on the gondola, via a universal-joint connetion, or a two degrees of freedom gimbal. This implies that there are two independent axes

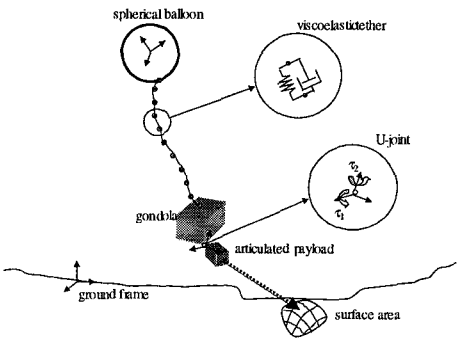

Fig. 1. Pointing dynamics model for a payload mounted on a gondola suspended from a balloon.

which need to be controlled to provide declination and azimuth of the payload, about the reference body triad represented by the gondola body axes. With the dynamics described above (i.e., payload and gondola dynamics, reaction wheel dynamics, and balloon and tether dynamics) the equations of motion are stronly coupled through centrifugal and Coriolis terms (gyroscopic forces). These forces are of small magnitude if sufficiently slow maneuvers take place, and providing the attitude of the gondola is only slightly perturbed from an equilibrium inertial orientation. Therefore, with standard sensing equipment located on board the gondola, i.e. three-axis accelerometers, gyro unit, and a global attitude determination system such as GPS or an on-board star tracker, both inertial position (in planetocentric coordinates), inertial attitude (with respect to the planetocentric reference frame, which is being propagated through ephemeris in the on-board computer) and their rates can be determined. Some estimation procedure is necessary when the full dynamic state cannot be measured. A previous paper by one of us has looked into the attitude estimation of the gondola using only accelerometer data.

With this information, the nonlinear gyroscopic terms can be cancelled from the equations. This results in a feedback linearized equation of motion in the direction of the controlled axes, namely we achieve near perfect state decoupling, and we can design the local controllers assuming independent control loops.

D. Simulations and Results

Next, we show some simulation results.

These results identify which are the issues affecting gondola stability, and which are the effects of wind changes which affect pointing.

II. Second Scenario: Flight Train Dynamic Stability Models of Balloon/Parachute Suspended Payload

Next, we derive some numerical models used to investigate the dynamics of several types of superpressure balloon

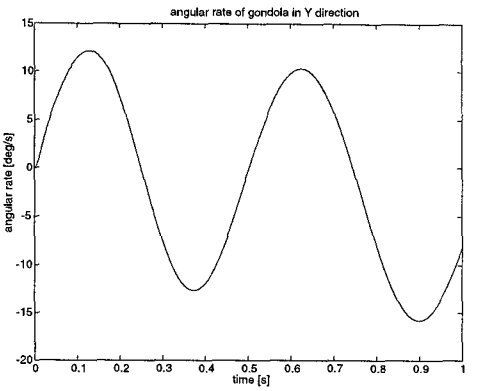

Fig. 2. Gondola angular rate vs. time.

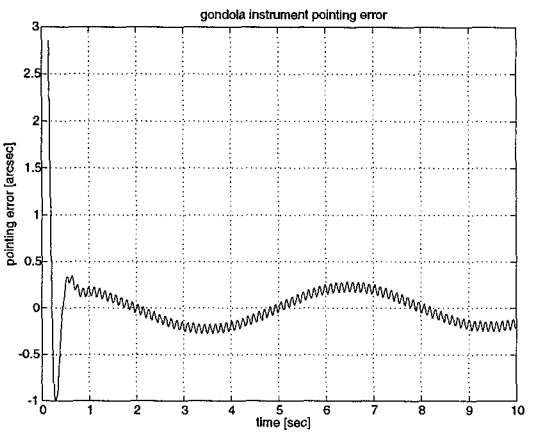

Fig. 3. Gondola instrument angular pointing error vs. time.

configurations: a balloon in wind tunnel, a balloon in free-fall, a balloon connected to a parachute in wind tunnel, a balloon connected to a parachute in free-fall, descent og a gondola under an inflating balloon. These models are able to determine the onset of dynamic instability (attributed to von Karman vortex shedding) as a function of design parameters such as: parachute diameter and riser length, balloon diameter, tether length, gondola mass ad inertia.

III. Conclusions

In this paper, we have documented the analysis, and testing done to assess the validity of models developed for Parachute/Balloon-assisted deployment of sensor packages within the Mars Aerobot Validation program at JPL. Two different scenarios are described: pointing dynamics and control of an articulated payload mounted on a balloon-supported gondola; the dynamics of various flight train configurations in different oscillatory regimes originated upon deployment. These scenarios have been motivated by the need to predict and validate flight-train stability behavior upon deployment before and after tests have been made. Details of these tests are also reported in this paper.

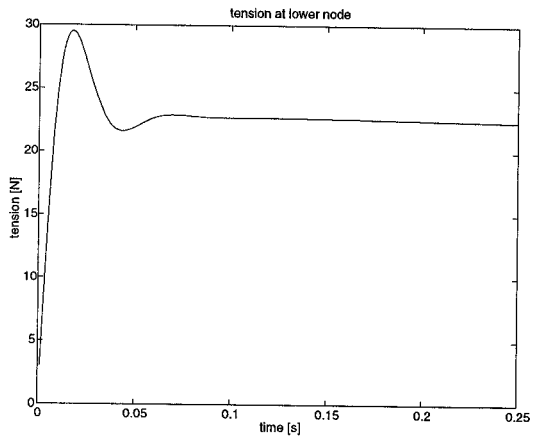

Fig. 4. tether tension vs. time.

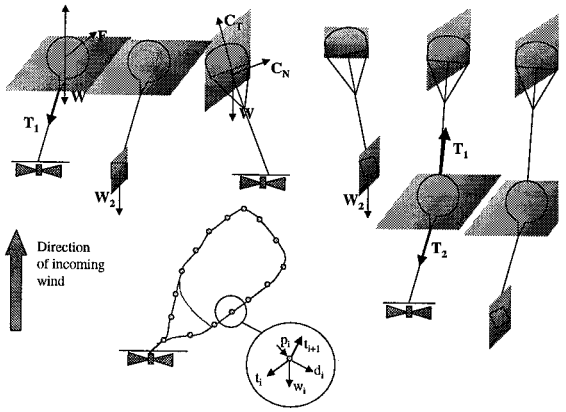

Fig. 5. Models of parachute/balloon flight trains to study dynamic instability during descent.

APPENDIX

A. The balloon in wind tunnel.

Following the nomenclature used in this paper, the equations of motion are given by:

$$\bar{m}^o \mathbf{a}^{\mathbf{B}+} \cdot \mathbf{t} = \mathbf{F}^{\mathbf{B}+} \cdot \mathbf{t} \quad (52)$$

$$\bar{m}^o \mathbf{a}^{\mathbf{B}+} \cdot \mathbf{n} = \mathbf{F}^{\mathbf{B}+} \cdot \mathbf{n} \quad (53)$$

$$I_b \ddot{\phi} = \mathbf{M}^{\mathbf{B}+} \cdot \mathbf{b_3} \quad (54)$$

where $\mathbf{a}^{\mathbf{B}+}$ is the acceleration of B+ with respect to O, $\mathbf{F}^{\mathbf{B}+}$ and $\mathbf{M}^{\mathbf{B}+}$ are the force and moment vector acting on body B, and $\mathbf{t}$ and $\mathbf{n}$ are the tangential and normal unit vector to the line of length L.

Defining the following quantities:

$$A = s\phi s\theta + c\phi c\theta \quad (55)$$

$$B = s\phi c\theta - c\phi s\theta \quad (56)$$

$$f_0 = r_b^2 AC/I_b \quad (57)$$

$$E = 1/(1 + M_1 r_b^2 B^2/I_b) \quad (58)$$

the tether tension is

$$T = E(M_1 L(\dot{\theta})^2 + M_1 A r_b \dot{\phi}^2 + (D_y + S_y)s\theta + (D_z + S_z + Bb)c\theta)$$

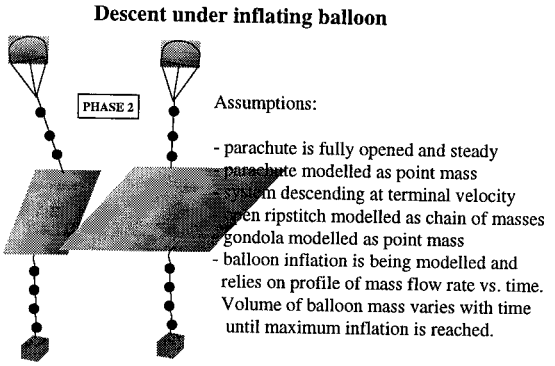

Fig. 6. Assumptions of descent under inflating balloon.

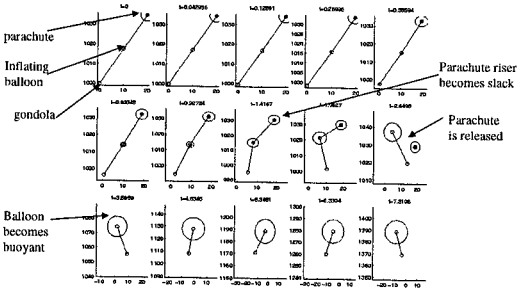

Fig. 7. Snapshots of parachute release when balloon becomes buoyant.

and the equations of motion are

$$\ddot{\theta} = F_{et}/(M_1 L) \quad (59)$$

$$\ddot{\phi} = torque/I_b \quad (60)$$

where

$$F_{et} = (D_y + S_y)c\theta - (D_z + S_z + Bb)s\theta \quad (61)$$

$$+M_1 r_b \dot{\phi}^2 B + M_1 f_0 T \quad (62)$$

$$torque = -r_b CT \quad (63)$$

Taking the limit as $r_b \to 0$, we obtain the equations for the point mass balloon. Figure ?? reports the tether tension vs. time when the percentage of Helium inside the envelope is 0.2. the wind speed is 3 m/s, the tether length is 3 m. Similar tests done in a wind tunnel at NASA LaRC show a response that closely matches the numerical results.

B. The balloon in free fall

When the balloon is in free fall, there are two additional degrees of freedom: the horizontal and vertical coordinates of the gondola. This point has been chosen as reference since all the inertial sensing instrumentation is located on the payload gondola. The situation is depicted in Figure ??. Defining m_g as the gondola-payload mass, and

$$L_2 = D_y + S_y \quad (64)$$

$$L_3 = D_z + S_z + Bb \quad (65)$$

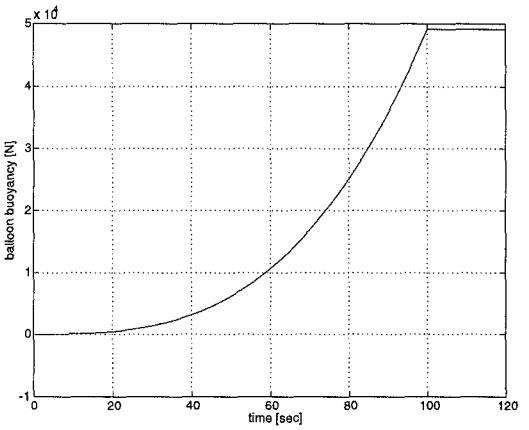

Fig. 8. Balloon buoyancy force during inflation process lasting 100 seconds.

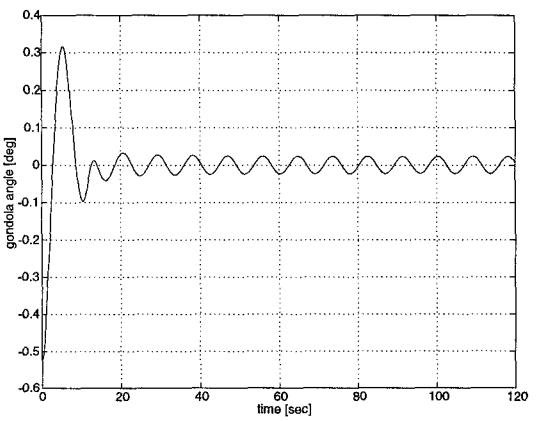

Fig. 9. Residual oscillation at gondola during inflation process lasting 100 seconds.

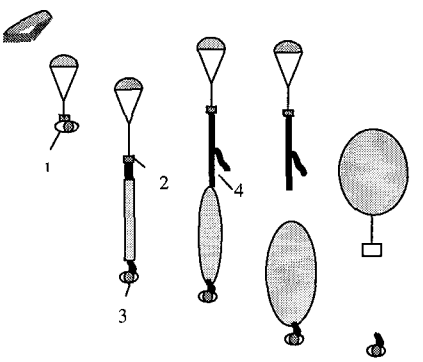

Fig. 10. Aerial Deployment and Inflation Concept. 1 - deployment module, 2 - balloon container, 3 -inflation system, 4 - ripstitch

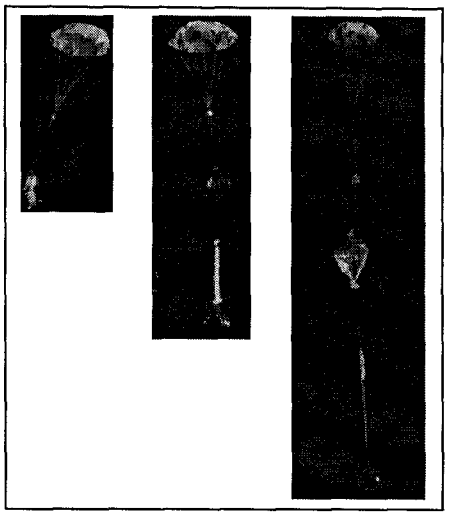

Fig. 11. Deployment and inflation of a 3 meter Mylar balloon.

the tether tension is

$$T = (1+\frac{\bar{m}r_b^2BC}{I_b}+\frac{\bar{m}}{m_g})^{-1}(L_3c\theta + L_2s\theta+\bar{m}(L\dot{\theta}^2+Ar_b\dot{\phi}^2+gc\theta))$$

and the equations of motion are

$$\bar{m}L\ddot{\theta} = L_2c\theta - L_3s\theta - \bar{m}(-r_b\dot{\phi}^2B-\frac{{r_b}^2ACT}{I_b}+gc\theta) \quad (66)(67)$$

$$I_b\ddot{\phi} = -r_bCT \quad (68)$$

$$m_g\ddot{y} = Ts\theta \quad (69)$$

$$m_g\ddot{z} = Tc\theta - m_pg \quad (70)$$

Figure ?? shows the behavior of the dynamic pressure, the Strouhal force, the tether tension, and the oscillation angle vs. time.

C. The balloon connected to the parachute in wind tunnel

When the parachute is connected to the balloon in the wind tunnel, the situation is as depicted in Figure ??. Here we model the parachute as a mass point. Therefore there is no inertia and fluid added inertia. Defining $\bar{m}_p$ as the parachute mass plus its added mass, L_{bg} the length of tether between balloon and ground, L_{pb} the length of tether between balloon and parachute, and

$$M_2 = D_{py}+L_{py} \quad (71)$$

$$M_3 = D_{pz}+L_{pz}-m_pg \quad (72)$$

the tension in the line connecting the balloon and the parachute is given by:

$$T_2 = (1+\frac{\bar{m}_pB^2}{\bar{m}})^{-1}((M_2s\phi+M_3c\phi)+\bar{m}_p(L_{pb}\dot{\phi}^2+AL_{bg}\dot{\theta}^2)+\frac{B\bar{m}_p}{\bar{m}}(L_2c\theta-L_3s\theta))$$

and the tension in the line connecting the ground to the balloon is given by:

$$T_1 = \bar{m}L_1\dot{\theta}^2 + (L_2c\theta - L_3s\theta) + BT_2$$

and the equations of motion are

$$\bar{m}L_{bg}\ddot{\theta} = (L_2c\theta - L_3s\theta) + BT_2 \quad (73)$$

$$\bar{m}_pL_{pb}\ddot{\phi} = -\frac{\bar{m}_pA}{\bar{m}}(L_2c\theta - L_3s\theta) + \quad (74)$$

$$(M_2c\phi - M_3s\phi) - \bar{m}_pL_{bg}\dot{\theta}^2B - \quad (75)$$

$$\frac{\bar{m}_pABT_2}{\bar{m}} \quad (76)$$

Figure ?? shows the behavior of the dynamic pressure, the Struohal force, the tehter tension, and the oscillation angle vs. time. The aerodynamic coefficients of the parachute (cruciform type) are shown in Figures ??, ??, and ??.

D. The balloon connected to the parachute in free fall

When the parachute is connected to the balloon in the free fall, the tether tensions are as follows:

$$T_1 = H_w(1 + \frac{H_wE_wA^2\bar{m}_p}{m_g})^{-1}(\Omega_1 + AE_w\Omega_2) \quad (77)$$

$$T_2 = E_w(\Omega_2 - \frac{\bar{m}_pAT_1}{m_g}) \quad (78)$$

where

$$E_w = (1 + \frac{\bar{m}_pB^2}{\bar{m}})^{-1}$$

$$H_w = (1 + \frac{\bar{m}}{m_g})^{-1}$$

$$\Omega_1 = L_2s\theta + L_3c\theta$$

$$\Omega_2 = -\frac{\bar{m}_pB}{\bar{m}}(L_2c\theta - L_3s\theta) + (M_2s\phi + M_3c\phi) + \bar{m}_p(AL_{bg}\dot{\theta}^2 + L_{pb}\dot{\phi}^2) + \bar{m}_pg(c\phi + Bs\theta))$$

The equations of motion then are:

$$m_g\ddot{y} = T_1s\theta \quad (79)$$

$$m_g\ddot{z} = T_1c\theta - m_gg \quad (80)$$

$$\bar{m}L_{bg}\ddot{\theta} = c\theta(L_2 + T_2s\phi) - \quad (81)$$

$$s\theta(l_3 + T_2c\phi) - \bar{m}gs\theta \quad (82)$$

and

$$\bar{m}_pL_{pb}\ddot{\phi} = (M_2c\phi - M_3s\phi) - \frac{\bar{m}_pA}{\bar{m}}(L_2c\theta - L_3s\theta) - \bar{m}_pBL_{bg}\dot{\theta}^2 + \frac{\bar{m}_p}{m_g}BT_1 - \frac{\bar{m}_p}{\bar{m}}ABT_2 + \bar{m}_pg(As\theta - s\phi)$$

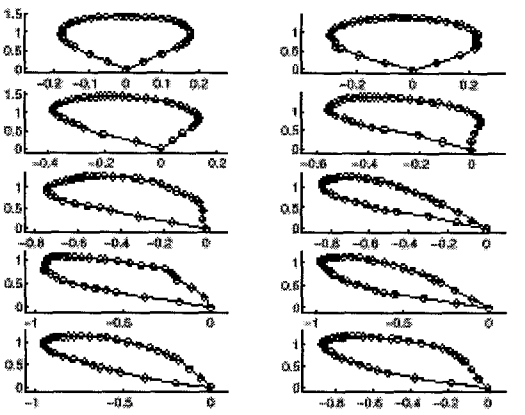

Fig. 12. Snapshots of dynamic simulation of the dynamics of a Helium filled deformable balloon exposed to wind tunnel airflow from below.

I. Fluid-structure interaction in a deformable balloon

The two-dimensional deformable balloon inmersed in a uniform airflow is shown in Figure ??. This model is used to estimate the tension in the envelope membrane when an airflow causes the balloon to deform. The airflow is from below the envelope, and the balloon is hinged to the ground at the base point. The balloon envelope is modelled by discretizing it in a series of point masses connected to each other by elastic springs. Tension in the springs is zero when the stretch is negative, i.e. the material of the balloon envelope does not support any compressive load.

The equations of motion are given by:

$$m_i\ddot{y}_i = T_ic\theta_i - T_{i-1}c\theta_{i-1} + F_{iy}$$

$$m_i\ddot{z}_i = T_is\theta_i - T_{i-1}s\theta_{i-1} + F_{iz}$$

$$T_i = EA\epsilon_i$$

$$\epsilon_i = (s_i - s_0)/s_0$$

$$s_i = \sqrt{(y_{i+1} - y_i)^2 + (z_{i+1} - z_i)^2}$$

$$F_{yi} = F_{Ni}s\theta_i + F_{ti}c\theta_i$$

$$F_{zi} = -F_{Ni}c\theta_i + F_{ti}s\theta_i$$

$$F_{Ni} = (q_iA_i)\mathbf{i_r} \cdot \mathbf{n_i}$$

$$F_{ti} = (q_iA_i)\mathbf{i_r} \cdot \mathbf{t_i}$$

$$q_i = \frac{1}{2}\rho((\dot{y}_i - U_y)^2 + (\dot{z}_i - U_z)^2)$$

where $\mathbf{i_r}$ is the unit vector along the relative flow.

Acknowledgement 1: The research described in this paper was carried out during the MABVAP (Mars AeroBot Validation Program) program at the Jet Propulsion Laboratory, California Institute of Technology, under a contract with National Aeronautics and Space Administration.

References

[1] A.E. Bryson, Jr., and Yu-Chi Ho, *Applied Optimal Control*, Hemisphere Publishing Corporation, New York, (Halstead Press/John Wiley & Sons), Revised Printing, 1975.

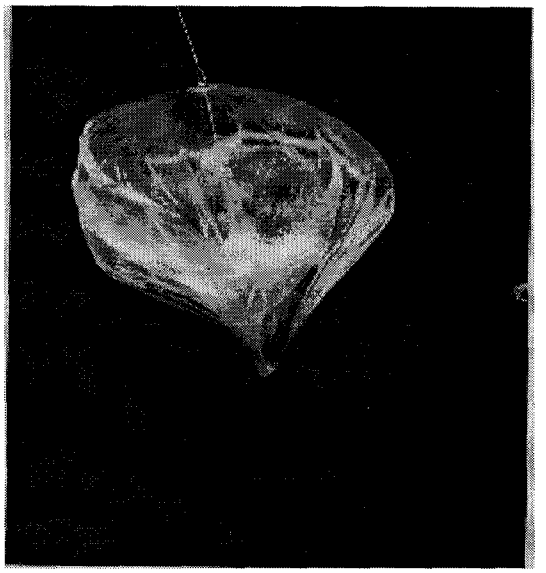

Fig. 13. Balloon Test in LaRC vertical wind tunnel (December 1997).

[2] D. Boussalis, "IRU Model CAB Update,", *Project Cassini Controls Analysis Book,* Jet Propulsion Laboratory, JPL D-9638, November 14, 1997.

[3] V.V.Kerzhanovich, J.Cutts, A.Bachelder, J.Cameron, J.Hall, J.Patzold, M.Quadrelli, A.Yavrouian, J.Cantrell, T.Lachenmeier, M.Smith, MARS AEROBOT VALIDATION PROGRAM, presented at the AIAA Balloon Technology Conference, 1999.